ELSEVIER

Journal of Fluids and Structures 20 (2005) 1127–1143

JOURNAL OF FLUIDS AND STRUCTURES

www.elsevier.com/locate/jfs

A model of wall pressure correlation for prediction of turbulence-induced vibration

S. Finnveden*, F. Birgersson[1], U. Ross, T. Kremer[2]

MWL, Aeronautical and Vehicle Engineering, KTH, SE-100 44 Stockholm, Sweden

Received 10 December 2003; accepted 26 May 2005

Abstract

The vibration response of a structure excited by a turbulent boundary layer is investigated experimentally and numerically. First, the wall pressure in a high speed acoustic wind tunnel is characterized and the cross-spectral density is approximated using a Corcos model with frequency dependent correlation lengths and a modified Chase model. Both models agree quite well with the measured cross spectrum. Second, based on these turbulence models, the vibration response is predicted and compared to measurements. At lower frequencies both models perform well. In a higher frequency region, however, the vibration response is greatest for length scales that are much longer than the one given by the convection velocity of the turbulence, and in this frequency region only the modified Chase model works effectively.

Keywords: Turbulence; Wall pressure; Correlation; Chase; Random vibration

1. Introduction

Vibration and noise in structures excited by turbulent boundary layer (TBL) flow has been, and continues to be, of interest in many engineering applications, e.g., piping systems, aircraft structures and marine applications. Reviews of the progress made within this area in the last 50 years are available in the literature (Bull, 1996; Schlichting, 1979; Blake, 1986; Leehey, 1988; Willmarth, 1975; Howe, 1991). Here, the vibration response of a thin plate to a TBL is investigated experimentally and numerically.

Turbulence is an intrinsically nonlinear process, which can only be expressed in statistical terms and is generally described by semi-empirical models. The quantity of interest for vibration prediction is the cross-spectral density of the wall pressure field. Early measurements of the wall pressure, e.g., by Corcos (1964) and Bull (1967), were analyzed based on the notion of a slowly changing pressure field that convects in the streamwise direction with a speed, the convection velocity, that is somewhat smaller than the free flow velocity. From these observations, the cross-spectral density could be represented as a function of similarity variables and, once Fourier transformed in space, the corresponding

*Corresponding author.
E-mail address: svantef@kth.se (S. Finnveden).
[1]Current address: Robert Bosch GmbH, Gasoline Systems, 70442 Stuttgart, Germany.
[2]Current address: Department for Lightweight Structures and Composite Materials, TU Darmstadt, 64287 Darmstadt, Germany.

0889-9746/$ - see front matter © 2005 Elsevier Ltd. All rights reserved.
doi:10.1016/j.jfluidstructs.2005.05.012

wavenumber frequency spectrum was found. This spectrum has a maximum at the convective peak, where the wavenumber equals the angular frequency divided by the convection velocity.

The perceived close fit to measured data in the space domain achieved by these earlier models is, however, deceptive. Most of the turbulent energy might indeed be given by pressure field components with wavenumbers around the convective peak, but these are not the components of greatest importance for the response of structures at frequencies above the aerodynamic coincidence. This coincidence occurs at the frequency when the structure's flexural wave speed equals the convection velocity, and around this frequency the largest vibration response is expected. At even higher frequencies and for moderate structural damping, the largest structural response has a characteristic length scale that is longer than the one that dominates the turbulence. Under these circumstances, it is the faster, low wavenumbers, or sub-convective components, that are largely responsible for the structural excitation, despite the fact that they contribute very little to the wall pressure.

With linear streamwise arrays of uniformly spaced and identical pressure transducers it is possible to filter out wavenumber components of the wall pressure cross spectrum. Measurements (Maidanik and Jorgensen, 1967; Blake and Chase, 1970; Farabee and Geib, 1991) taken in this way indicate a 'white' wavenumber spectrum in the sub-convective range. Another approach is to use a structure as a wavenumber filter, thus Martin and Leehey (1977) used a tensioned membrane, whereas Jameson (1975) used a clamped steel plate. There now exists some qualitative understanding of the wall pressure frequency spectrum in the low wavenumber domain, but there is still a lack of agreement regarding its magnitude.

Awareness of possible shortcomings of the Corcos model led to the development of a number of new models. Some of these (Efimtsov, 1982; Chase, 1980, 1987; Smol'yakov and Tkachenko, 1991; Ffowcs Williams, 1982) are compared by Graham (1997). The best model for high speed aircraft is, according to Graham, the one which provides an accurate description of the convective peak. Efimtsov's model, an extension of Corcos' model, is cited as a suitable candidate and will also be considered in this study. Some concerns regarding the multiplicative approach, upon which Corcos' and Efimtsov's models are based, are expressed. Graham concludes, however, that any further 'sophistication', as introduced by Chase, should only be necessary if the turbulence excited structure does not exhibit aerodynamic coincidence.

The conclusion from our study is that the correct modelling of only the convective peak may lead to gross errors ($\geqslant 10$ dB) in the predicted structural response at frequencies above the aerodynamic coincidence. This would therefore justify certain further 'sophistication', and Chase's model is a natural choice, given that it seems to represent the low wavenumber domain more accurately than other models (Borisyuk and Grinchenko, 1997). Some modifications were necessary to fit Chase's original model (Chase, 1980) to the measured data, and these are also reported herein.

The measurements of turbulence excitation were made in the acoustic wind tunnel at the Marcus Wallenberg Laboratory (MWL) and allowed for flow speeds up to 120 m/s, which is relatively high compared to most measurements found in the literature. Light weight accelerometers were used to measure the vibrational response of a clamped aluminum plate and two spatially separated microphones measured the wall pressure cross-spectral density.

The response to TBL excitation was calculated by a wavenumber frequency approach similar to that described in Birgersson et al. (2003), Maury et al. (2002), it is detailed by Birgersson (2003), Birgersson et al. (2005), Birgersson and Finnveden (2005). The response is thus given by a single integral, over the wavenumber domain, of the wavenumber frequency spectrum multiplied by the sensitivity function of the structure. This sensitivity function describes the response of the structure to a travelling pressure wave, and can be interpreted as a filter which only depends on the structure's geometrical and mechanical properties. If the sensitivity function is correct, any error in the estimated response will originate from an error in the wall pressure model. Thus, the wall pressure models can be assessed by the agreement between measured and predicted vibration response.

The major contribution of this work is the joint numerical and experimental evaluation of wall pressure and induced plate vibration at frequencies well above the aerodynamic coincidence. Several works, e.g., Birgersson et al. (2004), and Totaro and Guyader (2003) report on similar evaluations in situations where the Corcos model is good enough. The current work, however, provides an independent estimate of the parameters in the Chase model and, possibly, the first experimental confirmation of its ability to predict structural response at frequencies well above the aerodynamic coincidence.

The outline of this paper is as follows. Section 2 describes the measurements of the turbulent wall pressure. Section 3 presents the Corcos and Chase models of the wall pressure, together with modifications made to extend their validity over a greater frequency range. In Section 4 both modified models are compared to the measured wall pressure cross-spectral density. Also, the vibration response predictions based on the two models are compared to the measured response.

2. Measurements of turbulent wall pressure

The measurements had two purposes. The first of these was to determine the characteristics of the wall pressure field, while the second was to quantify the response of a flexible panel excited by this pressure field. The investigation was confined to frequencies below 5000 Hz because the plate vibration and plate emitted sound power at higher frequencies is relatively low.

2.1. Experimental set-up

The wind tunnel used for measurements is outlined in Fig. 1, and occupied all four measurement rooms of the MWL. The anechoic room functioned as a large silencer and as a plenum chamber. The fan system in the basement was capable of producing a maximum volume flow of about $10\,m^3\,s^{-1}$ and a pressure drop of 10 kPa. This system produced an overpressure in the anechoic room, which in turn provided a silent source of flow through the wind tunnel. In fact, when standing in the anechoic room, it was not possible to hear the fans, but only a rumbling from within the tunnel. The flow quality was good and the background noise level was below 25 dB(A).

The tunnel was a suspended 9 m long steel duct of rectangular cross-section with wall thickness 12 mm, height 175 mm and width 375 mm. The corners of the cross-section were rounded in order to avoid corner effects in the flow. The maximum flow velocity for the duct was 120 m/s.

Part of the tunnel was used as a test-section, with a horizontal aperture provided for the mounting of test panels. This section was located in a reverberation room, which made it relatively easy to determine the emitted sound power from any test panel. These measurements are not reported here. To minimize vibration of the test panels due to vibration of the duct, the duct wall was stiffened by two 40×40 mm steel bars both upstream and downstream from the test-section. Furthermore, a constrained damping layer was attached to the duct, further reducing the vibration level at high frequencies. Validation measurements proved the transmission of duct vibration to the test plates to be negligible (Finnveden, 2004).

The boundary layer thickness δ in the test-section was determined from hot wire measurements and theory given in Schlichting (1979), and was found to be sufficiently large for the intended measurements, without having to be triggered. Fig. 2 shows the measured velocity profile for a free flow velocity of 100 m/s. This measurement verifies that the velocity profile is as in a 'classical' boundary layer. Some other flow characteristics found from the measurements are given in Table 1.

A special plexiglas panel was used for TBL wall pressure measurements, as shown in Fig. 3 (left). Two moveable discs, to which microphones were mounted, were incorporated into the panel. The larger disk had a microphone (M1) flush-mounted at its centre, and this gave the reference pressure. The second, smaller disc was eccentrically mounted to the first, and had a second flush-mounted microphone (M2) attached. Rotation of the discs enabled the position of M2 on the panel, and its distance from M1, to be changed. The distance between the microphones could be varied between 13 and 130 mm, allowing a great variety of microphone positions for correlation measurements, and Fig. 3 (middle) shows the positions used in this study. However, it was later found that the positions close to the outer circle were contaminated by noise, probably caused by a small gap between the moveable parts, and the measurements taken at the three positions marked with crosses were therefore discarded. Small ($\frac{1}{8}$-in.) microphones, with their protection grids removed, were used in order to minimize the errors at high frequencies that are caused by finite microphone size.

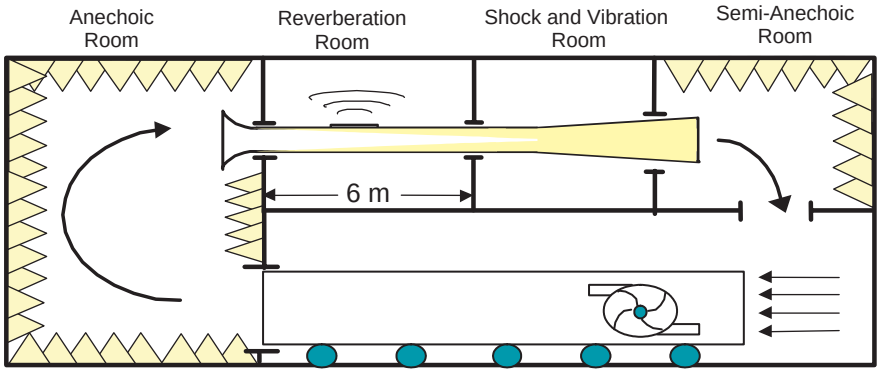

Fig. 1. Wind tunnel with test-section located in the reverberation room.

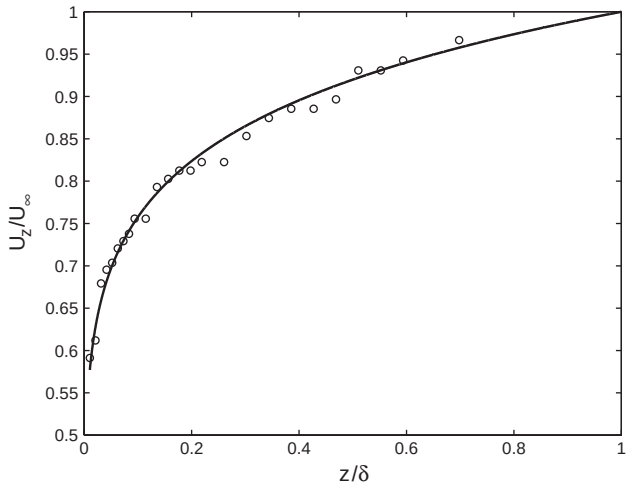

Fig. 2. Velocity profile for a free flow velocity of 100 m/s at a distance z from wall scaled with the boundary layer thickness δ. Circles are measured velocities and solid line corresponds to a power velocity distribution law (Schlichting, 1979) with $n = 8.3$.

Table 1
Estimated flow data from measurements

U_∞	80 (m/s)	100 (m/s)	120 (m/s)
δ (mm)	50	50	53
δ^* (mm)	5.1	5.2	5.5
U_c (m/s)	58	76	90
U_τ (m/s)	2.6	3.1	3.7

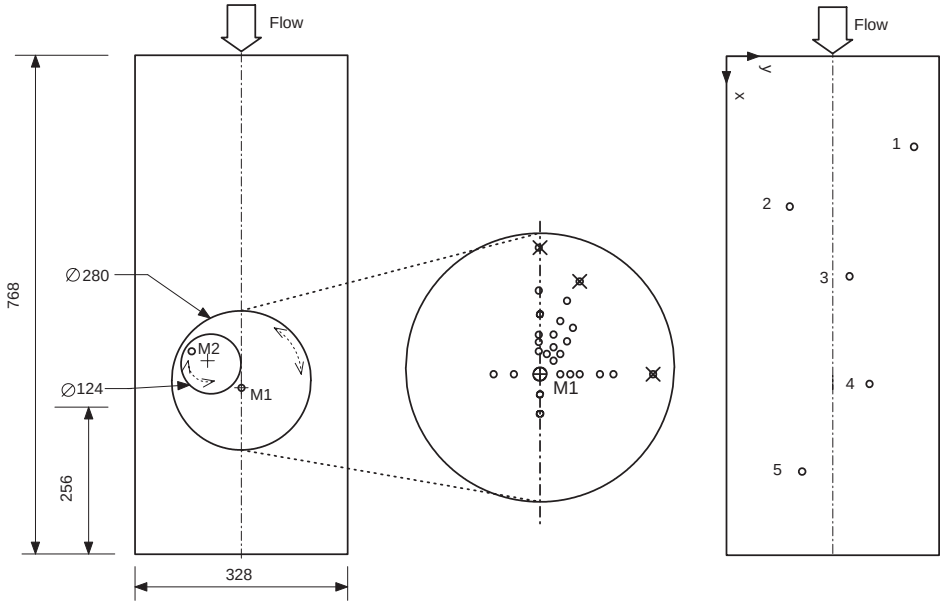

Fig. 3. Plexiglas plate (left) for wall pressure measurements with 26 measurement positions shown (middle) and aluminium plate with 5 accelerometer positions (right). Values are in mm.

The resolution of all auto spectra and coherence measurements was 6.25 Hz and the measurements were averaged for 1 min. This was not quite enough to bring out the coherent part of the signal for large microphone separation and for clarity the results shown are further averaged in swept 10% frequency bands. The validity of this approach was confirmed by a few narrow-band measurements with measurement times of over 1 h.

At frequencies below 150 Hz acoustic modes in the wind tunnel also had a noticeable effect on the measured pressure spectra. Noise cancellation techniques effectively reduced this effect, but in the context of this paper the removal of this 'contamination' is of little interest and is not reported here. All curve fitting to measured correlation data was performed in the frequency range from 250 Hz up to 3000 Hz, in which the data was considered to be the most reliable.

2.2. Wall pressure power spectral density

The double sided wall pressure power spectral density Φ_{pp} ($\mathrm{Pa}^2\,\mathrm{s/rad}$) was measured using a fixed microphone. Fig. 4 shows the wall pressure power spectral density plotted in dimensionless form for the three free flow velocities $U_\infty = 80, 100$ and $120\,\mathrm{m/s}$. As a comparison a reference curve (Robert, 1984), based on a collection of measurements in different wind tunnels, is also drawn. This reference is described by,

$$\frac{\Phi_{pp}U_\infty}{q^2\delta^*} = \begin{cases} 2.14\times10^{-5} & \omega\delta^*/U_\infty < 0.25, \\ 7.56\times10^{-6}\times(\omega\delta^*/U_\infty)^{-0.75} & 0.25 \leqslant \omega\delta^*/U_\infty \leqslant 3.5, \\ 1.27\times10^{-4}\times(\omega\delta^*/U_\infty)^{-3} & 3.5 < \omega\delta^*/U_\infty, \end{cases} \tag{1}$$

where ω is angular frequency and δ^* is displacement thickness. The dynamic pressure is given by $q = \rho_0 U_\infty^2/2$ with ρ_0 the density of the fluid. As is seen from the figure, this model describes the wall pressure power spectral density quite accurately with a small discrepancy of approximately 1 dB. Also, the measurements agree within 1–2 dB with the measurements collected by Keith et al. (1992). Other types of scaling with, for example, inner variables are available in the literature (Blake, 1986; Keith et al., 1992), but the one used was seen to give a reasonably good approximation of the data. What the model does not predict is the maximum value of the spectra at approximately $\omega\delta^*/U_\infty = 0.2$, which has been observed by other investigators as well, e.g. Farabee and Casarella (1991) and Leclercq and Bohineust (2002).

2.3. Wall pressure coherence

The cross-spectral density of the wall pressure is defined as

$$S_{pp}(\xi_1, \xi_2, \omega) = \langle p^*(x, y, \omega), p(x+\xi_1, y+\xi_2, \omega)\rangle, \tag{2}$$

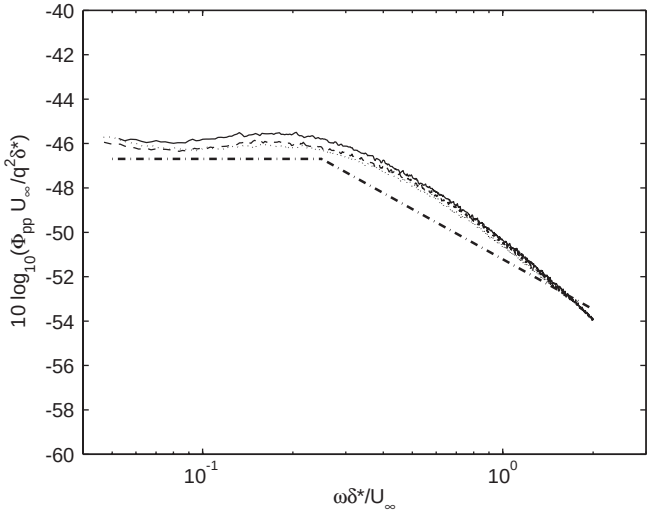

Fig. 4. Wall pressure power spectral density for three velocities: 80 m/s, solid; 100 m/s, dashed; 120 m/s, dotted. Reference curve proposed by Robert (1984) given as straight lines.

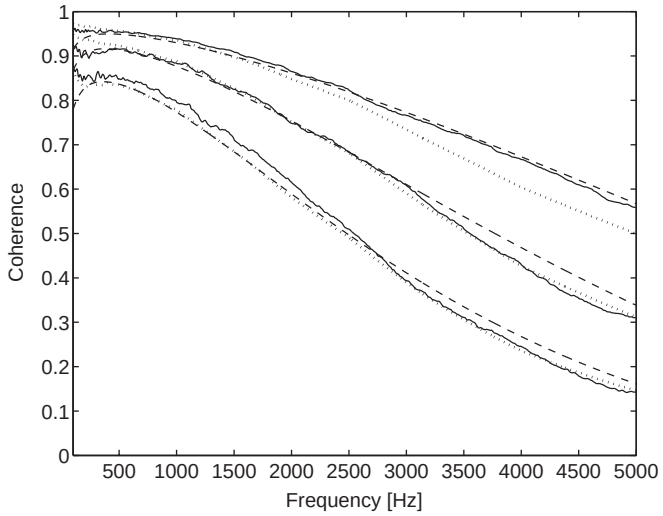

Fig. 5. Streamwise coherence as function of frequency. For 13 mm (top), 21 and 31 mm (bottom) streamwise separation. Solid, measurements; dashed, modified Chase; dotted, modified Corcos.

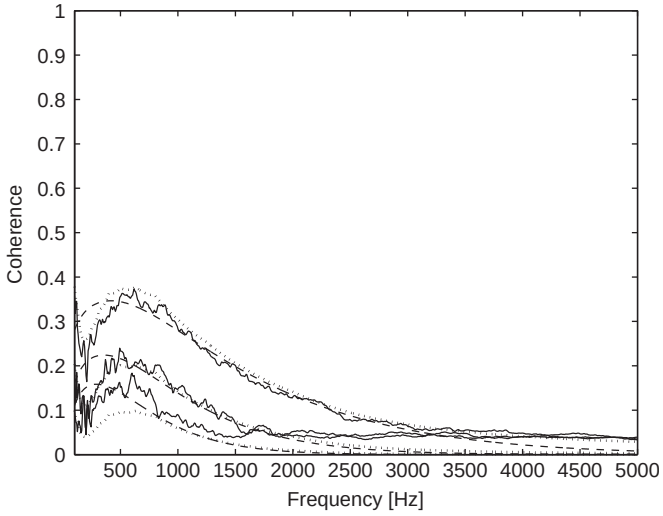

Fig. 6. Spanwise coherence as function of frequency. For 13 mm (top), 21 and 31 mm (bottom) spanwise separation. Solid, measurements; dashed, modified Chase; dotted, modified Corcos.

where p denotes wall pressure. $S_{pp}(\xi_1, \xi_2, \omega)$ can be expressed on the form

$$S_{pp}(\xi_1, \xi_2, \omega) = \Phi_{pp}(\omega)\Gamma(\xi_1, \xi_2, \omega), \tag{3}$$

where $\Phi_{pp}(\omega)$ is the wall pressure power spectral density and $\Gamma(\xi_1, \xi_2, \omega)$ describes the correlation between two points with a spatial separation of ξ_1 and ξ_2 in the longitudinal and transverse direction, respectively. $\Phi_{pp}(\omega)$ is here taken directly from the measurements, but it could also have been predicted, with an error of 1–2 dB, using Eq. (1). As in Farabee and Geib (1991), the modulus of the function Γ will be referred to as coherence, and its phase investigated separately. Note that sometimes, e.g. in Newland (1984), the coherence is denoted by the square of this modulus.

The wall pressure coherence was measured using two microphones with a spatial separation. Figs. 5 and 6 show measurements of streamwise and spanwise coherence, whereas Figs. 7 and 8 show the coherence given a spatial separation at an angle to the flow. Fig. 9 shows the measured phase of the cross-spectral density and Fig. 10 is a contour

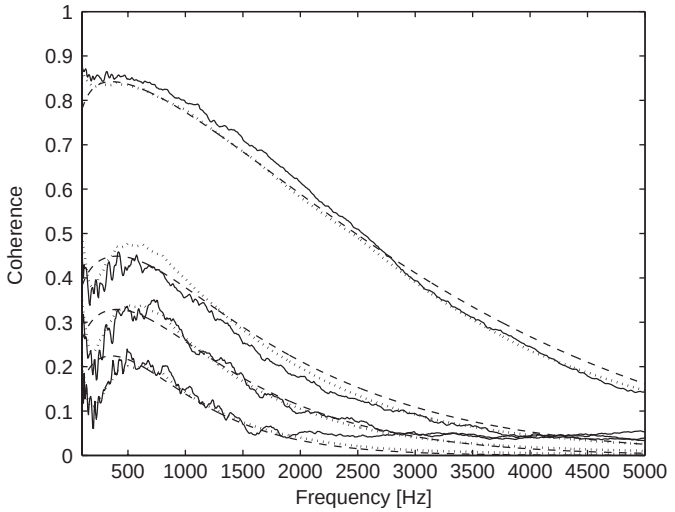

Fig. 7. Coherence on a quarter circle with 21 mm separation as function of frequency. Angle varies from 0° (top) to 90° (bottom). Solid, measurements; dashed, modified Chase; dotted, modified Corcos.

plot of measured coherence on a quarter circle. These results are used to assess the proposed models in the next section, and will be discussed in more detail then.

As noted in the literature, there is a relatively rapid loss in coherence at low frequencies, and noise cancellation techniques revealed this further by Farabee and Casarella (1991). Figs. 6 and 7 clearly exhibit a peak in the coherence spectrum when $\omega\delta/U_c \approx 2$. This phenomenon has recently been noted in, for example, Farabee and Casarella (1991), and was earlier observed by Bull (1967). However, Bull reported it as a levelling off to a constant value at frequencies below a cut off frequency given by $\omega\delta/U_c \approx 2.7$.

In conclusion, a wall pressure data base is collected. The generality of the measurement set up has been verified by hot wire measurements showing a classical turbulent boundary layer velocity profile. Also, the measured auto spectra agree within 1–2 dB with spectra found in other wind tunnels. Finally, correlation lengths estimated for a Corcos model agree with results from the literature, as will be shown in the next section.

3. Models for the cross-spectral density of the pressure

To calculate turbulence induced structural response it is important to have an accurate description of the cross-spectral density of the pressure. In this section Corcos' model is recapitulated, as Corcos' curve fit to measured narrow band pressure correlations (Corcos, 1964) is quite well established. However, experimental evidence suggests that Corcos' model overpredicts levels at wavenumbers below the convective peak [e.g., Martin and Leehey (1977), Chase (1980)]. As will be shown later, this was also evident in the present study and a modified Chase model was derived in order to best describe both measured turbulent wall pressure and plate response.

3.1. Modified Corcos model

Corcos assumed that the loss of coherence between two spatially separated points is equal to the loss of coherence in the streamwise direction multiplied by the loss of coherence in the spanwise direction. From a curve fit for the narrow-band spatial correlation between wall pressures, Corcos obtained

$$\Gamma(\xi_1, \xi_2, \omega) = \mathrm{e}^{-\alpha_1 k_c|\xi_1|}\,\mathrm{e}^{-\alpha_2 k_c|\xi_2|}\,\mathrm{e}^{\mathrm{i}k_c\xi_1}, \tag{4}$$

where

$$k_c = \omega/U_c. \tag{5}$$

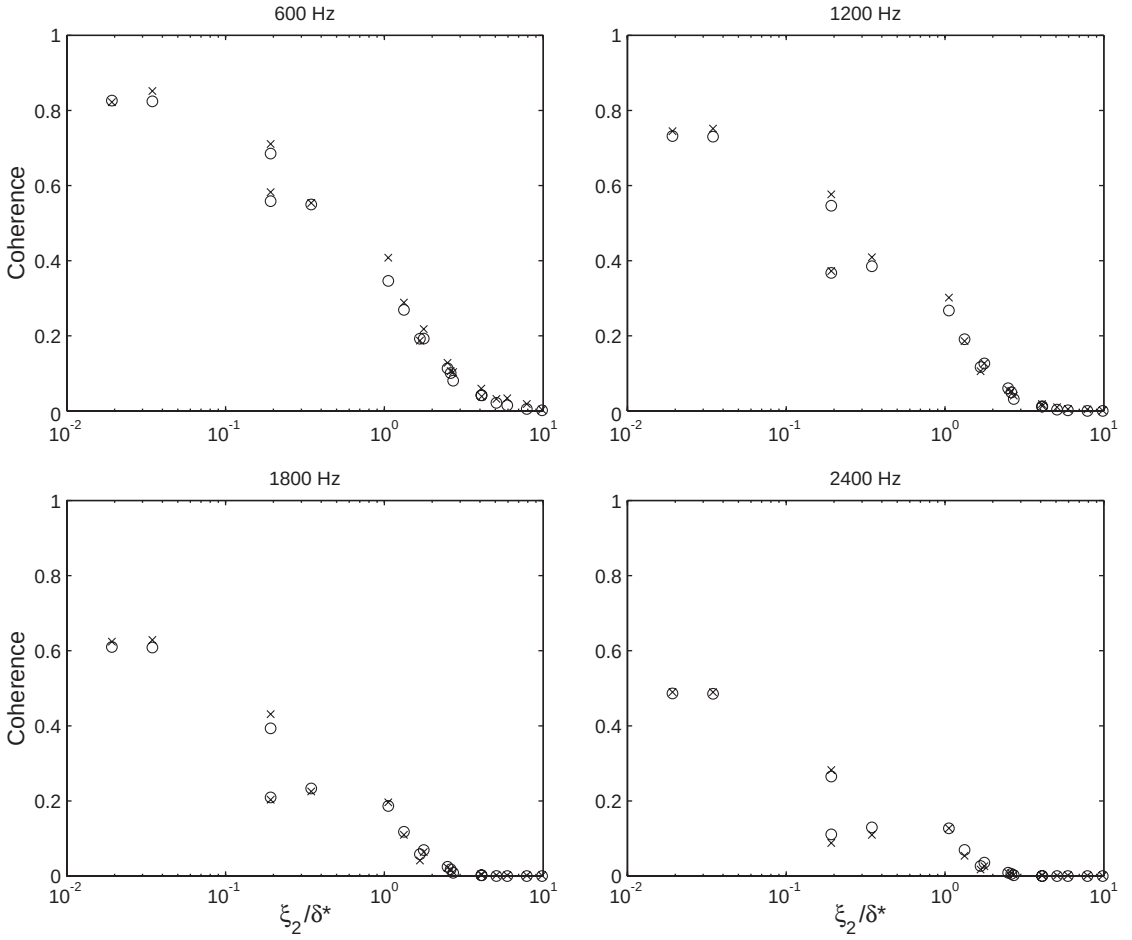

Fig. 8. Coherence at 600–2400 Hz for 16 points with varying spanwise and streamwise separation, shown as function of spanwise separation. '×', measurements; 'o', modified Chase. *Note*: points at the same spanwise separation can have different coherence depending on their streamwise separation.

The convection velocity U_c is thus given by the cross-spectral phase. It has a small tendency to be larger for large streamwise separations. Also, it has some dependence of frequency. In this study, however, a constant value for each flow speed is used.

The parameters α_i denote loss of coherence in the longitudinal and transverse directions. Various values are given in the literature for α_i; Blake (1986) for example recommends that $\alpha_1 = 0.116, \alpha_2 = 0.7$ be taken for smooth walls. These parameters may also be estimated directly from measurements. Following a similar philosophy as Efimtsov (1982), they can be considered as functions of frequency.

The wavenumber spectrum is found from a Fourier transform according to

$$P(k_1, k_2, \omega) = \frac{1}{(2\pi)^2} \int_{-\infty}^{+\infty} \int_{-\infty}^{+\infty} \Gamma(\xi_1, \xi_2, \omega) \mathrm{e}^{-\mathrm{i}k_1\xi_1} \, \mathrm{e}^{-\mathrm{i}k_2\xi_2} \, \mathrm{d}\xi_1 \, \mathrm{d}\xi_2, \tag{6}$$

and Corcos' model (4) can therefore be expressed in the wavenumber domain as

$$P(k_1, k_2, \omega) = \frac{\alpha_1 \alpha_2}{\pi^2 k_c^2 (\alpha_3^2 + (k_2/k_c)^2)(\alpha_1^2 + (k_1/k_c - 1)^2)}. \tag{7}$$

With just one set of parameters (α_1, α_2), Corcos' model did not describe the measured coherence over the entire frequency range. Hence, the model was modified by introducing one set for each third octave band and for each flow

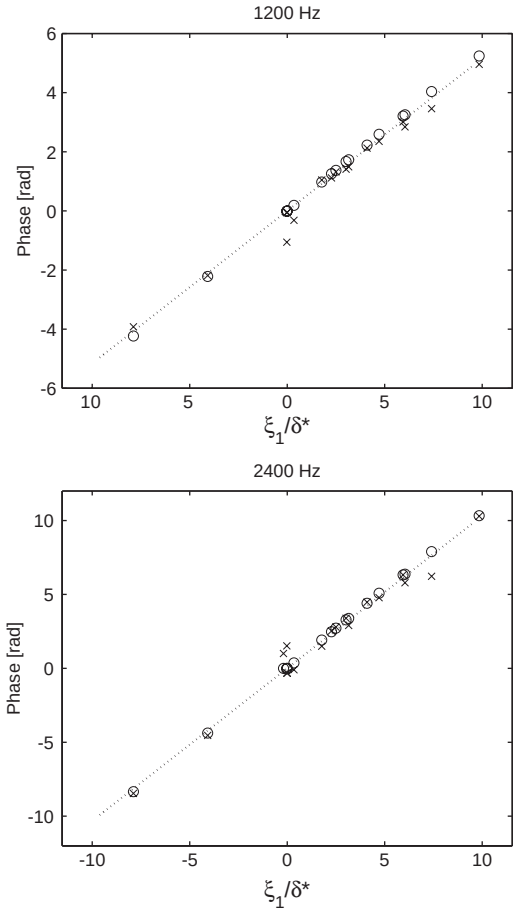

Fig. 9. Phase of pressure cross-spectral density for 16 points with varying spanwise and streamwise separation, shown as function of streamwise separation; '×', measurements; 'o', modified Chase; dotted line, Corcos.

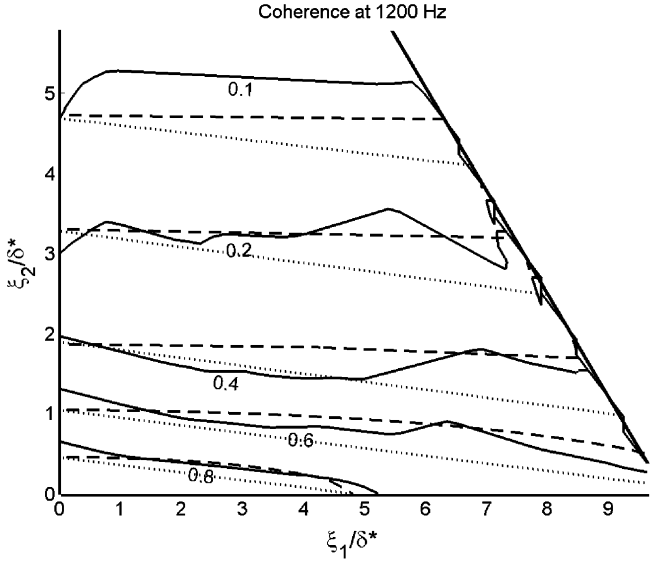

Fig. 10. Coherence contours at 1200 Hz as function of separation on a quarter circle. Solid, measurements; dashed, modified Chase; dotted, modified Corcos. No measurement points were located in the upper right corner.

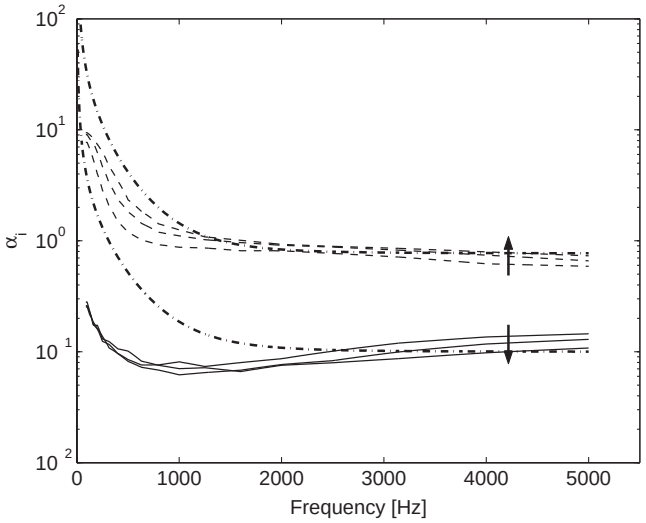

Fig. 11. Parameters α_i used in Corcos model and estimated in third octave bands. Solid, α_1; dashed, α_2; dash-dotted, α_i calculated for $U_\infty = 100\,\mathrm{m/s}$ with formula given by Efimtsov (1982). Arrows indicate increased flow speed.

velocity. That a modification of this kind is important can be seen from Fig. 11, where α_1 and α_2 are shown to vary from values of 0.3 and 9 down to values of 0.07 and 0.7, respectively. These values were found by applying a multidimensional unconstrained nonlinear minimization routine to the difference between predicted and measured wall pressure coherence in one-third octave bands. A linear interpolation between the values at centre frequencies was then made in order to define the parameters as continuous functions. It was possible to find values for one frequency at a time, but the values obtained were not as smooth. The α_i also depend on flow velocity as indicated by the arrows, and having to estimate values for every third octave band naturally imposes a significant limitation on the modified Corcos model. An alternative, and computationally less expensive, method of estimating the constants is therefore desirable. Fig. 11 also shows the α_i calculated from Efimtsov's empirical expressions (Efimtsov, 1982) using his prescribed constants and $U_\infty = 100\,\mathrm{m/s}$. At high frequencies Efimtsov's values are quite close to the optimized values, but at low frequencies at least two of his seven constants, namely a_2 and a_5, need to be decreased.

3.2. Modified Chase model

Chase's model is believed to describe the low-wavenumber domain ($k_1 \ll k_c$) better than Corcos' model, which is important for the response prediction later. In his model, Chase also predicts the wall pressure auto spectrum $\Phi_{pp}(\omega)$, which was here already known from measurements (or from Eq. (1)). This quantity was therefore factored out and not considered in what follows. Chase's original model (Chase, 1980, Eqs. 72–74) gave a reasonable, but not quite satisfactory, description of the measured cross-correlation. Nevertheless, investigations showed that the predicted cross-correlation could be improved with some small adjustments, as shown in that which follows. As Chase neglected some terms when presenting his model in the space domain, the more precise version given by Josserand et al. (1989, Eqs. (12), 14a–14c) is used

$$\Gamma(\xi_1, \xi_2, \omega) = \mathrm{A}_M(\omega)\mathrm{f}_M(\xi_1, \xi_2, \omega)\mathrm{e}^{-z_M}\,\mathrm{e}^{\mathrm{i}\,k_c\xi_1} + \mathrm{A}_T(\omega)\mathrm{f}_T(\xi_1, \xi_2, \omega)\mathrm{e}^{-z_T}\,\mathrm{e}^{\mathrm{i}\,k_c\,\xi_1}, \tag{8}$$

where

$$\mathrm{f}_M = 1 + z_M + \alpha_M^2\,\mu_M^2\left(1 - z_{M1}^2/z_M\right) + 2\mathrm{i}\alpha_M\,\mu_M\,z_{M1}, \tag{9}$$

$$\mathrm{f}_T = 1 + z_T + \alpha_T^2\left(1 - z_{T2}^2/z_T\right) + \alpha_T^2\,\mu_T^2\left(1 - z_{T1}^2/z_T\right) + 2\mathrm{i}\alpha_T\,\mu_T\,z_{T1}, \tag{10}$$

$$z_{M1} = \mu_M\alpha_M k_c\xi_1, \quad z_{T1} = \mu_T\alpha_T k_c\xi_1, \tag{11}$$

$$z_{M2} = \alpha_M k_c, \xi_2, \quad z_{T2} = \alpha_T k_c\xi_2, \tag{12}$$

$$\alpha_M = \sqrt{1 + (b_M k_c \delta)^{-2}}, \quad \alpha_T = \sqrt{1 + (b_T k_c \delta)^{-2}}, \tag{13}$$

$$z_M = \sqrt{z_{M1}^2 + z_{M2}^2}, \quad z_T = \sqrt{z_{T1}^2 + z_{T2}^2}. \tag{14}$$

For the modified model two more parameters $\gamma_{M,T}$ are introduced in order to better fit the transverse length scale used in Eq. (12) to the measurements, such that

$$z_{M2} = \gamma_M \alpha_M k_c \xi_2, \quad z_{T2} = \gamma_T \alpha_T k_c \xi_2. \tag{15}$$

This changes f_T slightly to become

$$\mathrm{f}_T = 1 + z_T + \alpha_T^2 \gamma_T^2 \left(1 - z_{T2}^2 / z_T\right) + \alpha_T^2 \mu_T^2 \left(1 - z_{T1}^2 / z_T\right) + 2\mathrm{i}\alpha_T \mu_T z_{T1}. \tag{16}$$

In the modified model, Eqs. (15)–(16) therefore replace Eqs. (10) and (12).

The relative magnitudes $A_{M,T}$ proposed by Josserand and Lauchle (1989) could have been used in the model. However, preliminary investigations showed that they have a greater dependence on flow speed than is indicated in that paper. The following model is therefore postulated:

$$\begin{aligned} A_M(\omega, U_c) &= (1 - r)/\left(1 + \alpha_M^2 \mu_M^2\right), \\ A_T(\omega, U_c) &= r/\left(1 + \alpha_T^2 \gamma_T^2 + \alpha_T^2 \mu_T^2\right) \end{aligned} \tag{17}$$

with

$$\begin{aligned} r(\omega, U_c) &= a - b\omega/\omega_0, \\ \omega_0 &= 10^5 [\mathrm{rad/s}], \quad 0 \leqslant r \leqslant 1. \end{aligned} \tag{18}$$

This modified model will be used in the next section.

The wavenumber frequency spectrum corresponding to the modified model is given by

$$P(k_1, k_2, \omega) = a_M k_1^2 K_M^{-5} + a_T (k_1^2 + k_2^2) K_T^{-5} \tag{19}$$

with

$$K_i^2 = \frac{(\omega/(1 - \mu_i^2) - U_c k_1)^2}{(U_c^2 \mu_i^2/(1 - \mu_i^2))} + k_1^2 + \left(\frac{k_2}{\gamma_i}\right)^2 + (b_i \delta)^{-2},$$

$$a_i = \frac{3 A_i k_c (\alpha_i / \sqrt{1 - \mu_i^2})^3}{\pi \gamma_i \mu_i}, \quad i = M, T. \tag{20}$$

This spectrum is quite similar to the one given by Chase (1980, Eqs. 68–70). The factor $(1 - \mu_i^2)$ arises, in a similar way to that found by Josserand and Lauchle (1989) if the approximation $\mu_i \ll 1$ is not made, and the introduction of γ_i in Eq. (15) results in a scaling of k_2 in K_i. If $\mu_i \ll 1$ and $\gamma_i = 1$, the presented spectrum equals the one given by Chase.

The modified Chase model is defined by Eqs. (8)–(18), excluding Eqs. (10) and (12), and the set of parameters in Table 2. A similar minimization routine as for the modified Corcos model was used to find these parameters. The scale of the problem was larger this time, with as many as 12 nondimensional parameters for the three free flow velocities. In order to accomplish this, first the seven parameters μ_i, b_i, γ_i and r were determined for each flow velocity and each

Table 2
Parameters for modified Chase model

U_∞	80 (m/s)	100 (m/s)	120 (m/s)
a	0.5362	0.5928	0.6468
b	0.1869	0.1355	0.1382

b_M	b_T	μ_M	μ_T	γ_M	γ_T
0.5973	0.3158	0.2831	0.0614	1.2267	1.4186

third-octave band. A closer inspection of these parameters revealed that only r varied noticeably. The parameters a and b were then introduced instead of r, and the averaged values for the other parameters gave a good first guess to curve fitting for all flow velocities and all frequencies.

The resulting parameter set is the one reproduced in Table 2. It is interesting to compare these values to the values given by Chase (1980, Eq. (86): $\mu_M = \mu_T = 0.176, \gamma_M = \gamma_T = 1, b_T = 0.378$ and $b_M = 0.756$). The values for $b_{M,T}$ are not greatly different from the ones found here, however, μ_M is almost twice as large, whereas μ_T on the other hand is approximately three times smaller. Thus the length scale in the spanwise and streamwise direction has a ratio of approximately 4 in the first term of Eq. (8) and 23 in the second term. Using Chase's parameters, the ratio is approximately 6 in both terms. Values of $\gamma_{M,T}$ close to unity in Table 2 might have raised questions as to the necessity of introducing these variables, but they lay in the approximate range of 1.2–1.4 and did, in fact, allow for a much better fit to the measured data. Chase prescribed two functions C_M and C_T, which are almost independent of flow speed. In the modified model, the functions A_M and A_T are introduced instead. These functions depend on a, b, and therefore significantly on flow speed. According to Chase, the first term in Eq. (8) gives the mean flow-turbulence contribution to the wall pressure, whereas the second term gives the turbulence–turbulence contribution, and it does not seem unreasonable that the relative contribution of the latter term should increase with flow speed.

4. Assessment of models

In this section the modified Corcos and Chase models described earlier will be put to the test. Firstly, they have to accurately describe the measured wall pressure cross-spectral density and secondly, they have to enable a satisfactory prediction of turbulence induced structural response.

4.1. Comparison with measured wall pressure

A comparison of the measured cross-spectral density of the pressure with the predicted results from a modified Chase and Corcos' model will be presented here. Only the results for a free flow velocity of 100 m/s will be shown, as these results were representative of the other two velocities and the difference in measured and predicted coherence was more or less the same for all three velocities.

When optimizing the parameters for these two models, a curve fit to the measured cross-spectral density was made as described in Section 3. Figs. 5–10 show how these models agree with the measured coherence and phase. Where applicable, solid lines represent measurements in the figures, whereas dashed and dotted lines represent the modified Chase and Corcos models, respectively.

Figs. 5 and 6 show the streamwise and spanwise coherence, for a spatial separation of 13, 21 and 31 mm. Generally, the coherence decreases with increasing separation and frequency. Below a cut off frequency of approximately 500 Hz there is, however, a levelling off to a constant value in Fig. 5, whereas a maximum in the coherence is visible in Fig. 6 around this frequency.

From Fig. 6 it is obvious that the measured coherence had a threshold level of 0.04, below which the coherence could not be observed. This threshold level arises from the limited measurement time of 1 min for each separation and can be considered as noise. To decrease this level to a lower value a measurement time of the order of 1 h or more is recommended, and some later measurements were carried out with this longer time span. For the optimization process any measured value of the coherence below 0.04 was not used.

Fig. 7 shows the coherence on a quarter circle with 21 mm separation as a function of frequency. Four angles are investigated in the figure: 0°, 20°, 40° and 90°. As was seen in the previous figures, the measured and predicted coherence agree surprisingly well and there is little difference in accuracy between the modified Corcos and modified Chase model.

Fig. 8 shows the coherence as a function of the spanwise separation at 16 measurement points, which has different spanwise and streamwise separations. During the optimization procedure it was found that the average difference between predicted and measured coherence was approximately 0.02 and the figure seems to support this observation.

The phase of the cross-spectral density is displayed in Fig. 9. The Corcos model assumes a convected phase given by $\omega\xi_1/U_c$, which in the figure is a straight line. The Chase model predicts a phase very close to this line and the measurements confirm that the assumption of a phase convected downstream with a single convection velocity is not too bad. Some measurements with zero separation in the ξ_1 direction should optimally have a phase close to zero according to the models, but nonetheless show a phase in the figure. This behaviour was attributed to the increased measurement errors that occur for large spanwise separations, where the coherence is very small and the phase is erratic.

Fig. 10 is an attempt to compare the measured and predicted coherence in space at 1200 Hz. The solid contours were linearly interpolated from a set of 21 measurement points on a quarter circle and the level curves extend from 0.8 down to 0.1. The dashed and dotted lines are the contours that a Chase or Corcos like model might predict for the coherence at this frequency. The main difference between them is that Chase's model has elliptic curves as compared to the straight lines given by Corcos' model. With the limited measurement points available, it is hard to determine which model is the more representative from this observation alone, but more measurement points might possibly give some clues as to this. Some recent numerical simulations (Singer, 1996) seem to suggest a better fit to elliptical curves, thus supporting the use of a Chase or a Smol'yakov and Tkachenko model.

Reviewing all the figures it is obvious that both models provide for a reasonably good description of the measured wall pressure cross-spectral density. To decide which is the more suited from this type of measurement would be difficult, and would require a much larger number of measurement points with long measurement times. Furthermore the separation distance should be increased, which in turn demands much from the measurement equipment and wind tunnel set-up. Instead, a different approach will be followed in the next paragraph, where the vibrational response of a turbulence excited plate is predicted using the two models and the results are compared to measurements to decide their applicability.

4.2. Vibrational response

The characteristics of the investigated aluminum plate were as follows: length L_x 76.8 cm, width L_y 32.8 cm, thickness h 1.6 mm, Young's modulus $E = 7 \times 10^{10}\,\mathrm{N/m^2}$, density $\rho = 2700\,\mathrm{kg/m^3}$ and a Poisson ratio v of 0.33. For the response predictions, the plate was assumed to be clamped along all edges.

Under operation there is a pressure difference between the inside and outside of the wind tunnel. Thus, the plate is statically deflected by as much as 4.0 mm at its centre and it becomes pre-stressed. The response of a pre-stressed simply supported plate was predicted showing that the effect was mainly to shift the resonance frequencies slightly upwards, especially at lower frequencies. For the third octave band powers, however, the effect was only of the order of 1 dB or less and therefore these results are not commented further here.

The plate's damping loss factor was estimated in octave bands from decay rate measurements for the three free flow velocities and is given in Table 3. Thus, under operation of the wind tunnel, a shaker gave an additional excitation to the plate. Then, the exciter was suddenly removed from the plate and the initial decay of the vibration velocity was monitored. It was not easy to estimate the reverberation time in this way and to get more confidence in the damping estimate, the vibration response of the plate under operation was measured with a fine frequency resolution so that the resonances' 3-dB bandwidth could be estimated. This procedure confirmed the decay rate measurements but showed also that there is a large spread in damping between the modes, most probably as their radiation efficiency varies a lot.

The auto spectral density of the velocity S_{vv} of the plate can either be found from (Newland, 1984)

$$S_{vv}(\mathbf{r},\mathbf{r},\omega) = \omega^2 \int_{\infty} |G(\mathbf{r},\boldsymbol{\alpha},\omega)|^2 \mathrm{S}_{PP}(\boldsymbol{\alpha},\omega)\,\mathrm{d}\boldsymbol{\alpha}, \tag{21}$$

or equivalently using a Fourier series expansion, e.g. Birgersson et al. (2003),

$$S_{vv}(\mathbf{r},\mathbf{r},\omega) = \omega^2 \sum_m \sum_n |G(\mathbf{r},\boldsymbol{\alpha}_{mn},\omega)|^2 S_{PP}(\boldsymbol{\alpha}_{mn},\omega), \tag{22}$$

where $\boldsymbol{\alpha}_{mn} = (m\pi/L_x, n\pi/L_y)$. S_{PP} is a Fourier transform, Eq. (21), or a Fourier series expansion, Eq. (22), of the wall pressure cross-spectral density given by Eq. (3). The sensitivity function G is the response of the clamped plate at

Table 3
Measured loss factor in octave bands

Octave band (Hz)	80 (m/s)	100 (m/s)	120 (m/s)
125	0.010	0.045	0.065
250	0.007	0.006	0.011
500	0.005	0.006	0.005
1000	0.004	0.005	0.004
2000	0.003	0.003	0.004

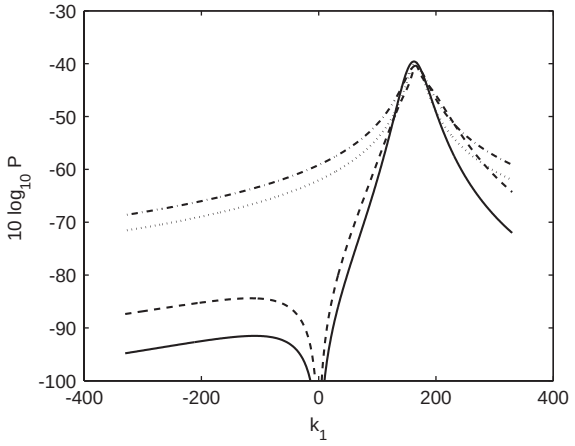

Fig. 12. Wavenumber frequency representation of the wall pressure cross correlation with modified Chase (dashed) and modified Corcos (dotted) at 2000 Hz and for $k_2 = 0$. As a comparison original Chase (solid) and Corcos (dash–dotted).

location $\mathbf{r} = (x, y)$ to a travelling pressure wave of the form $p(\mathbf{s}, \boldsymbol{\alpha}_{mn}, \omega) = \mathrm{e}^{-\mathrm{i}\alpha_m s_x}\,\mathrm{e}^{-\mathrm{i}\alpha_n s_y}\mathrm{e}^{\mathrm{i}\omega t}$. Eq. (22) is computationally more efficient and was used for the calculations.

The sensitivity function was evaluated with a spectral finite element method (SFEM) similar to the one presented by Birgersson et al. (2003). A merger of this method with a standard FEM was made in order to model clamped plates, as described by Birgersson (2003), Birgersson et al. (2005), and Birgersson and Finnveden (2005).

In Fig. 12, the wavenumber frequency spectra $P(k_1, 0, \omega)$ at 2000 Hz are compared for some of the models discussed. This is a convenient way to visualize the low wavenumber differences that are present below the convective peak. Above the aerodynamic coincidence frequency the structural modes will become increasingly excited by the low wavenumbers of the wall pressure spectra, and the difference of approximately 10 dB in this region between the modified Corcos and Chase models will be strongly reflected in the response spectra of the turbulence excited structure. The 'original' models are shown as a comparison. Corcos' model has a constant set of parameters, ($\alpha_1 = 0.116, \alpha_2 = 0.7$), and Chase's model (Chase, 1980, Eqs. 68–70) is used in combination with the values presented by Chase (1980), i.e., $\mu_{M,T} = 0.176, b_T = 0.378$ and $b_M = 0.756$. Corcos' model with Efimtsov's values for α_i gave more or less the same result as the modified Corcos for this frequency. The modified Corcos model is approximately 3 dB lower than the 'original' in the low wavenumber domain, which gave a small, but not sufficient, improvement to the response predictions shown later.

A nondimensional metric R for the response of the plate was defined as

$$R = \frac{\omega^2 \rho^2 h^2 S_{vv}}{\Phi_{pp}}, \tag{23}$$

and Fig. 13 shows the calculated and measured metric R for the three free flow velocities in averaged $\frac{1}{3}$-octave bands. The response is an average of the response at five positions of the plate, as given in Table 4. The response calculated using the modified Chase model is still not perfect, with an average error of 3 dB in the third octave bands. It does, however, represent a great improvement on the modified Corcos model and to the authors' knowledge the accuracy of the predicted plate response is one of the best to be found in the literature.

If the sensitivity function is correct, any error in the predicted response should originate from an error in the wall pressure model. However, the computational model is built on a number of assumptions about the plate, e.g., that all edges are rigidly clamped and that there is no static pre-stress induced by the pressure difference between the two sides of the plate, and errors in these assumptions will produce errors in the subsequent predictions. The significance of these errors was investigated by determining the effect of changing the boundary conditions to simply supported, and of including pre-stress from a measured static deflection. The total effect of these changes on the predicted response was around 3 dB or less. Predictions from both wall pressure models would have been affected in the same way by the changes, and therefore it is believed that these modelling errors would not have changed the conclusions that have been drawn from the work.

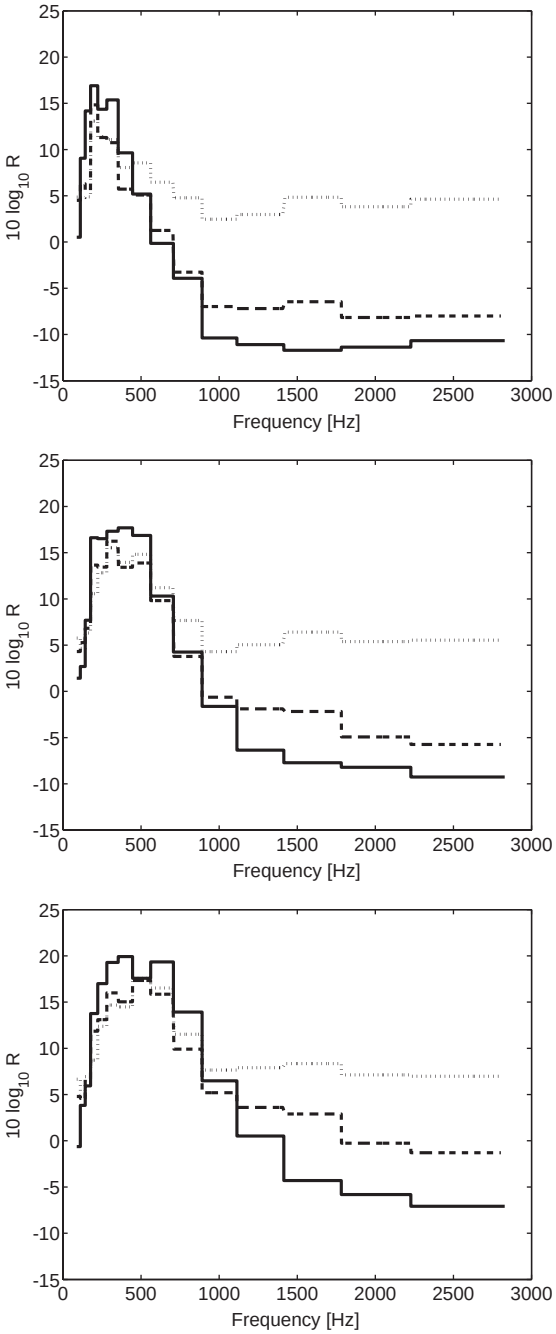

Fig. 13. Nondimensional vibration response in 1/3-octave bands for a clamped plate with a free flow velocity of 80 m/s (top), 100 m/s (middle) and 120 m/s (bottom). Solid, measurements; dashed, results based on modified Chase; dotted, results based on modified Corcos.

5. Conclusion

This investigation acquired a database on the wall pressure cross-spectral density beneath a turbulent boundary layer. The wind tunnel used had a small cross-sectional dimension, but was on the other hand unaffected by fan noise and allowed for high flow speeds. The results were obtained over an extended frequency range and a number of spatial

Table 4
Positions of measured and predicted plate response

x (m)	0.134	0.224	0.334	0.499	0.634
y (m)	0.284	0.089	0.184	0.229	0.119

Note: Plate is located in the xy-plane with origo placed in one corner.

separations. The main focus was to find an accurate model of the measured cross-spectral density, that also allowed for a satisfactory prediction of the vibrational response of turbulence excited plate structures.

A number of models to describe the cross-spectral density are readily available in the literature. Here, Corcos' and Chase's models were applied to the measured data. However, they were, in their original form, not suited to modelling the behaviour of the cross spectra over the whole frequency range and therefore they were modified slightly. In a manner similar to the Efimtsov model, the parameters in the Corcos model were made frequency and flow speed dependent. In Chase's model, two parameters were introduced to better fit the spanwise coherence to the measurements, which decayed quicker than predicted by the original model. Also the relative amplitude of the term describing the mean shear–turbulence contribution to the one describing the turbulence–turbulence contribution to the wall pressure was made frequency and flow speed dependent.

Both turbulence models agree with the measured coherence, typically the error is below 0.02. Due to a limited measurement time the coherence had a threshold level of approximately 0.04 below which it was not possible to detect any coherent signals. This makes it difficult to discriminate between the turbulence models based on the wall pressure measurements alone. Later, the cross spectra for a few points were averaged over more than an hour and this showed that it is possible to reduce the threshold level by at least a factor of 10.

The vibration response of a thin-walled plate mounted in the wind tunnel was measured and also predicted using the wall pressure models. Both models agree with the measured vibration response in a lower frequency regime, with a typical error of 3 dB. Above the aerodynamic coincidence, however, only the modified Chase model is correct, and a difference of approximately 10 dB was found between the models. To the best of the authors' knowledge, the current study provides the first experimental verification of the superiority of Chase type models over Corcos type models in predicting vibration response at frequencies well above the aerodynamic coincidence.

Acknowledgements

This work was supported by the European Commission, ENABLE (GRD4_CT-00-00223) and the Swedish Research Council (621-2002-5661). The authors are grateful to Arne Johansson, Gustav Amberg, Dan Henningsson, Gilles Robert and John Fitzpatrick for helpful discussions and to Roger Halkyard for reading the manuscript and suggesting improvements.

References

Birgersson, F., 2003. Prediction of random vibration using spectral methods. Ph.D. Thesis, KTH MWL, TRITA-AVE 2003:30.

Birgersson, F., Finnveden, S., 2005. A spectral super element for modelling of plate vibration: part 2, turbulence excitation. Journal of Sound and Vibration 287, 315–328.

Birgersson, F., Ferguson, N.S., Finnveden, S., 2003. Application of the spectral finite element method to turbulent boundary layer induced vibration of plates. Journal of Sound and Vibration 259, 873–891.

Birgersson, F., Finnveden, S., Robert, G., 2004. Modelling turbulence induced vibration of pipes with a spectral finite element method. Journal of Sound and Vibration 278, 749–772.

Birgersson, F., Finnveden, S., Nilsson, C.-M., 2005. A spectral super element for modelling of plate vibration: part 1, general theory. Journal of Sound and Vibration 287, 297–314.

Blake, W.K., 1986. Mechanics of Flow-Induced Sound and Vibration, vol. II. Academic Press, New York.

Blake, W.K., Chase, D.M., 1970. Wavenumber frequency spectra of turbulent boundary-layer pressure measured by microphone arrays. Journal of the Acoustical Society of America 49, 862–877.

Borisyuk, A.O., Grinchenko, V.T., 1997. Vibration and noise generation by elastic elements excited by a turbulent flow. Journal of Sound and Vibration 204, 213–237.

Bull, M.K., 1967. Wall pressure fluctuations associated with subsonic turbulent boundary layer flow. Journal of Fluid Mechanics 28, 719–754.

Bull, M.K., 1996. Wall-pressure fluctuations beneath turbulent boundary layers: some reflections on forty years of research. Journal of Sound and Vibration 190, 299–315.

Chase, D.M., 1980. Modelling the wavevector-frequency spectrum of turbulent boundary layer wall-pressure. Journal of Sound and Vibration 70, 29–67.

Chase, D.M., 1987. The character of the turbulent wall pressure spectrum at subconvective wavenumbers and a suggested comprehensive model. Journal of Sound and Vibration 112, 125–147.

Corcos, G.M., 1964. The structure of the turbulent pressure field in boundary layer flows. Journal of Fluid Mechanics 18 (3), 353–378.

Efimtsov, B.M., 1982. Characteristics of the field of turbulent wall pressure fluctuations at large Reynolds numbers. Soviet Physics—Acoustics 28 (4), 289–292.

Farabee, T.M., Casarella, M.J., 1991. Spectral features of wall pressure fluctuations beneath turbulent boundary layers. Physics of Fluids A 3, 2410–2420.

Farabee, T.M., Geib, F.E., 1991. Measurements of boundary layer pressure fluctuations at low wavenumbers on smooth and rough walls. ASME Symposium on Flow Noise Modelling, Measurement and Control, NCA-vol. 11, FED-vol. 130, pp. 55–68.

Ffowcs Williams, J.E., 1982. Boundary-layer pressures and the Corcos model: a development to incorporate low-wavenumber constraints. Journal of Fluid Mechanics 125, 9–25.

Finnveden, S., 2004. Evaluation of modal density and group velocity by a finite element method. Journal of Sound and Vibration 273, 51–75.

Graham, W.R., 1997. A comparison of models for the wavenumber frequency spectrum of turbulent boundary layer pressures. Journal of Sound and Vibration 206, 541–565.

Howe, M.S., 1991. Surface pressures and sound produced by turbulent flow over smooth and rough walls. Journal of the Acoustical Society of America 95, 1041–1047.

Jameson, P.W., 1975. Measurement of the low wavenumber component of turbulent boundary layer pressure spectral density. Fourth Biennal Symposium on Turbulence in Liquids, University of Missouri-Rolla, USA.

Josserand, M.A., Lauchle, G.C., 1989. Errata: D.M. Chase JSV 1980. Journal of Sound and Vibration 128, 519–523.

Keith, W.L., Hurdis, D.A., Abraham, B.M., 1992. A comparison of turbulent boundary layer wall-pressure spectra. ASME Journal of Fluids Engineering 114 (2), 338–347.

Leclercq, D.J.J., Bohineust, X., 2002. Investigation and modelling of the wall pressure field beneath a turbulent boundary layer at low and medium frequencies. Journal of Sound and Vibration 257, 477–501.

Leehey, P., 1988. Structural excitation by a turbulent boundary layer: an overview. ASME Journal of Vibration Acoustics Stress, and Reliability in Design 110, 220–225.

Maidanik, G., Jorgensen, D.W., 1967. Boundary wave-vector filters for the study of the pressure field in a turbulent boundary layer. Journal of the Acoustical Society of America 42, 494–501.

Martin, N.C., Leehey, P., 1977. Low wave number wall pressure measurements using a rectangular membrane as a spatial filter. Journal of Sound and Vibration 52, 95–120.

Maury, C., Gardonio, P., Elliott, S.J., 2002. A wavenumber approach to modelling the response of a randomly excited panel, part I: general theory. Journal of Sound and Vibration 252, 83–113.

Newland, D.E., 1984. An Introduction to Random Vibration and Spectral Analysis. Longman, New York.

Robert, G., 1984. Modélisation et simulation du champ excitateur induit sur une structure par une couche limite turbulente, École Centrale de Lyon, Ph.D. Thesis nr. 8402.

Schlichting, H., 1979. Boundary Layer Theory, seventh ed. McGraw-Hill, New York.

Singer, B.A., 1996. Turbulent wall pressure fluctuations: new model for off-axis cross-spectral density. NASA Contractor Report 198297.

Smol'yakov, A.V., Tkachenko, V.M., 1991. Model of a field of pseudonic turbulent wall pressures and experimental data. Soviet Physics–Acoustics 37 (6), 627–631.

Totaro, N., Guyader, J.-L., 2003. Model of Frequency Averaged Injected Power into a Plate Excited by a Turbulent Boundary Layer. Acta Acustica United with Acustica 89 (4), 647–657.

Willmarth, W.W., 1975. Pressure fluctuations beneath turbulent boundary layers. Annual Review of Fluid Mechanics 7, 13–28.